

Cite this: DOI: 10.1039/xxxxxxxxxx

Honey, I shrunk the bubbles: microfluidic vacuum shrinkage of lipid-stabilized microbubbles[†]

Vaskar Gnyawali,^{*ade} Byeong-Ui Moon,^{*ade} Jennifer Kieda,^{bde} Raffi Karshafian,^{cde} Michael C. Kolios,^{cde} and Scott S. H. Tsai^{†ade‡}

Received Date

Accepted Date

DOI: 10.1039/xxxxxxxxxx

www.rsc.org/journalname

We present a microfluidic technique that shrinks lipid-stabilized microbubbles from $O(100)$ to $O(1)$ μm in diameter—the size that is desirable in applications as ultrasound contrast agents. We achieve microbubble shrinkage by utilizing vacuum channels that are adjacent to the microfluidic flow channels to extract air from the microbubbles. We tune a single parameter, the vacuum pressure, to accurately control the final microbubble size. Finally, we demonstrate that the resulting $O(1)$ μm diameter microbubbles have similar stability to microfluidics generated microbubbles that are not exposed to vacuum shrinkage. We anticipate that, with additional scale-up, this simple approach to shrink microbubbles generated microfluidically will be desirable in ultrasound imaging and therapeutics applications.

Microbubbles are used in a variety of clinical applications, ranging from imaging, diagnostics, to therapeutics.^{1–3} Microbubbles in these applications are generally injected intravenously, where they flow in the blood stream and circulate throughout the body.³

In ultrasound imaging applications, microbubbles exposed to low amplitude ultrasound pulses undergo linear and non-linear oscillations, emitting strong ultrasound echo signals.³ Signals from the echos increase the image contrast, thereby improving the visual distinction between blood and the surrounding tissues.⁴ This improvement leads to increased detection sensitivity, and accuracy of imaging, facilitating enhanced detection of thrombosis

and diseased tissues.^{5–7}

Ultrasound and microbubbles have also been utilized for therapeutics such as in enhancing gene and drug delivery.^{8,9} Delivery occurs through pores on the membrane of tumor cells to lyse the cells or selectively deliver genes and/or drugs for cancer treatment^{10–12} and enhanced endocytosis.¹³

The acoustic response of microbubbles depends on the microbubbles' characteristics such as their size and shell-type, in addition to the degree of ultrasound exposure. Therefore, monodisperse (uniform characteristics) microbubbles are more desirable than polydisperse (non-uniform characteristics) microbubbles in many biomedical applications. Sub-micron control of bubble production has also the potential of generating nanobubbles (typically 550 nm or less), a burgeoning field in ultrasound contrast and therapy.¹⁴ Both microbubbles and nanobubbles can also be used therapeutically,¹⁵ and control over size is an important factor in their efficacy as microbubble behavior critically depends on size.¹⁶ However, producing monodisperse microbubbles that have the length-scales relevant to biomedical ultrasound remains challenging.

In the aforementioned applications, the microbubbles required are typically 1–7 μm in diameter.^{5,17} Conventional methods used to generate these microbubbles such as sonification,¹⁸ high shear emulsification,¹⁹ inkjet printing,²⁰ and coaxial electrohydrodynamic atomization (CEHDA),²¹ create polydisperse microbubbles at bubble diameters below 10 μm .^{17,18,21} As a result of the microbubbles' polydispersity, filtration steps are needed to attain microbubbles of the desired size. Inkjet printing of microbubbles achieves better control of microbubble sizes, but the approach is limited to generating liquid or volatile solvent filled bubbles.^{17,18} The commercially available and U.S. Food and Drug Administration (FDA) approved DEFINITY[®] microbubbles are polydisperse microbubbles with an average diameter of 1–3 μm , but some bubbles can be as large as 20 μm in diameter.²²

While microfluidic techniques produce monodisperse microbubbles with excellent size-control,^{17,22–25} microfluidics gen-

^a Department of Mechanical and Industrial Engineering, Ryerson University, Toronto, Canada.

^b Department of Electrical and Computer Engineering, Ryerson University, Toronto, Canada.

^c Department of Physics, Ryerson University, Toronto, Canada.

^d Institute for Biomedical Engineering, Science and Technology (iBEST), Toronto, Canada.

^e Keenan Research Centre, St. Michael's Hospital, Toronto, Canada.

[†] Electronic Supplementary Information (ESI) available: [details of any supplementary information available should be included here]. See DOI: 10.1039/b000000x/

* Equal contribution authors.

‡ scott.tsai@ryerson.ca

erated microbubbles have lower limits of size that directly depend on the dimensions of the bubble generating microchannel orifice.²² Generating microbubbles that are on the relevant length-scale for biomedical ultrasound and therapeutics applications either requires complex-to-manufacture phase-change nanoparticles²⁶ or microfluidic orifice widths that are on the order of just a few micrometers. Fabricating microfluidic molds with such small orifices is expensive and requires high-resolution photolithography.¹⁷ This makes a simple and low-cost alternative microfluidic approach that produces small microbubbles highly desirable.

In this Communication, we describe a simple approach to shrink bubbles generated from a conventional microfluidic flow focusing orifice into microbubbles that are on the relevant length-scale for ultrasound and therapeutics applications. The novelty of our approach is in our embedded vacuum microchannels adjacent to the main liquid-filled microchannel that microbubbles flow through.²⁷ By tuning a single parameter, the vacuum pressure in the adjacent microchannels, we controllably shrink microbubbles in the main liquid channel to as small as sub-micrometer diameters. We anticipate that the simplicity of our approach will make it potentially useful to the biomedical ultrasound community, and also open up new avenues of applications for microbubbles.

We use air as the dispersed gaseous phase. The continuous liquid phase is a mixture of lipids, glycerol (Sigma Aldrich Corporation, St. Louis, MO, USA), and pluronic F-68 (Fisher Scientific, Pittsburgh, PA, USA) in a 1:1:1 volumetric ratio. The lipid solution is prepared using 9:1 molar ratio of 1,2-distearoyl-sn-glycero-3-phosphocoline (DSPC) (Avanti Polar Lipids, Alabaster, AL, USA) and 1,2-distearoyl-sn-glycero-3-phosphoethanolamine-N [methoxy-(polyethylene glycol)-5000] (DSPE-PEG5000) (Avanti Polar Lipids, Alabaster, AL, USA) in saline (lipid concentration of 1.5 mg/mL). The composition of the lipids is similar to the FDA-approved and commercially available DEFINITY[®] microbubbles.²⁸ The interfacial tension of the continuous phase mixture and air is 1.5 mN/m, measured using the pendant drop method.²⁹ We note that this continuous phase mixture is also used in the medical ultrasound literature to stabilize perfluorocarbon droplets, which are vaporized in animal models for potential applications in contrast-enhanced imaging and drug delivery.³⁰

We pattern a single-layer polydimethylsiloxane (PDMS, Sylgard 184 silicone elastomer kit, Dow Corning, Midland, MI, USA) slab using conventional soft lithography techniques.³¹ Briefly, on a silicon wafer, we spin-coat a 80 μm thick film of SU-8 2075, which is then patterned by UV light through a photomask that is designed with a computer-aided design (CAD) software (AutoCAD 2010, Autodesk, Inc., Dan Rafael, CA, USA) and printed on a transparency sheet (25 400 dpi, CAD/ART Services Inc., Bandon, OR, USA). The pattern formed on the wafer by photolithography is transferred to the PDMS. Inlets for air, lipid solution, and vacuum, and the outlet, on the PDMS slab are opened using a 1 mm diameter biopsy punch (Integra Miltex, Inc., Rietheim-Weilheim, Germany). The PDMS slab is then irreversibly bonded to a glass microscope slide using oxygen plasma (Harrick Plasma, Ithaca, NY, USA) to complete the microfluidic chip (Fig. 1a).

Fig. 1b shows the flow focusing orifice with a width of 20 μm . The channel immediately downstream of the orifice has a width

of 200 μm (Fig. 1a). Even further downstream, the serpentine channel has a width of 350 μm and a total length of 350 mm. Two vacuum inlets on the two sides of the device supply vacuum pressure to the microfluidic device via interdigitated microchannels that are patterned adjacent to the serpentine channel (Fig. 1a). The interdigitated vacuum channels have widths of 150 μm and are separated by a distance of 175 μm from the serpentine channel. All channels have height $h = 80 \mu\text{m}$.

We supply pressurized air to the air inlet of the device through a control valve using Tygon tubing (Saint gobain S.A., Courbevoie, France). The control valve (Omega Engineering Inc., Norwalk, Connecticut, USA) is coupled to a pressure gauge (Omega Engineering Inc., Norwalk, Connecticut, USA) to control the air pressure at the air inlet. We use an inlet air pressure, $P_a = 4$ psi, in all of our experiments. The continuous liquid phase containing the lipid solution is supplied by a constant flow rate syringe pump (Harvard Instruments, Holliston, MA, USA) at a flow rate, $Q = 4 \mu\text{L}/\text{min}$. Microbubbles pinch-off at the flow focusing orifice (Fig. 1b), and flow into the serpentine section of the microchannel, where the vacuum pressure from the vacuum microchannels cause the microbubbles to shrink continuously until they reach the outlet (Figs. 1c - 1f). In our experiments, we tune the vacuum pressure $P_v = 0$ to -90 kPa. We use a Mityvac hand vacuum pump (Mityvac, St. Louis, MO, USA) with an integrated pressure gauge to supply the vacuum pressure, and connect the pump to the interdigitated vacuum microchannels using Tygon tubing. A flow diagram of this experimental setup is available in Supplementary Information.[†]

We use an inverted microscope (Olympus Corp., Tokyo, Japan) and an attached high speed camera (Phantom M110, Vision Research, Wayne, NJ, USA) to capture experimental images of the microbubbles. The camera operates at 100 fps with an exposure time of 500 μs . Using ImageJ software, we measure the initial microbubble diameter, D_i , immediately after they are generated at the orifice (Fig. 1b). Subsequently, we measure the final microbubble diameter, D_f , at a fixed location in the serpentine microchannel near the outlet of the device (Fig. 1f).

The microbubbles generated at the orifice have initial diameters, D_i , that are larger than the microchannel height $h = 80 \mu\text{m}$, which causes the microbubbles to be confined to a discoid shape. However, the vacuum-shrunk microbubbles near the outlet of the microfluidic device have diameters $D_f < h$, resulting in unconfined spherical microbubbles. To make an equivalent comparison of initial and final microbubble sizes, we convert our measurements to the initial and final volumes of the microbubbles, V_i and V_f , respectively, to determine the amount of microbubble shrinkage. See Supplementary Information for details about the conversion (which are based on equations we used in a recent paper³²).[†]

Figs. 1b-1f show representative experimental images of microbubbles at different locations in the serpentine microfluidic channel downstream of the bubble generating orifice. The microbubbles shrink as they flow downstream towards the outlet. These images are taken from an experiment where the applied vacuum pressure $P_v = -50$ kPa. A representative video of the microbubble shrinkage process is available in Supplementary

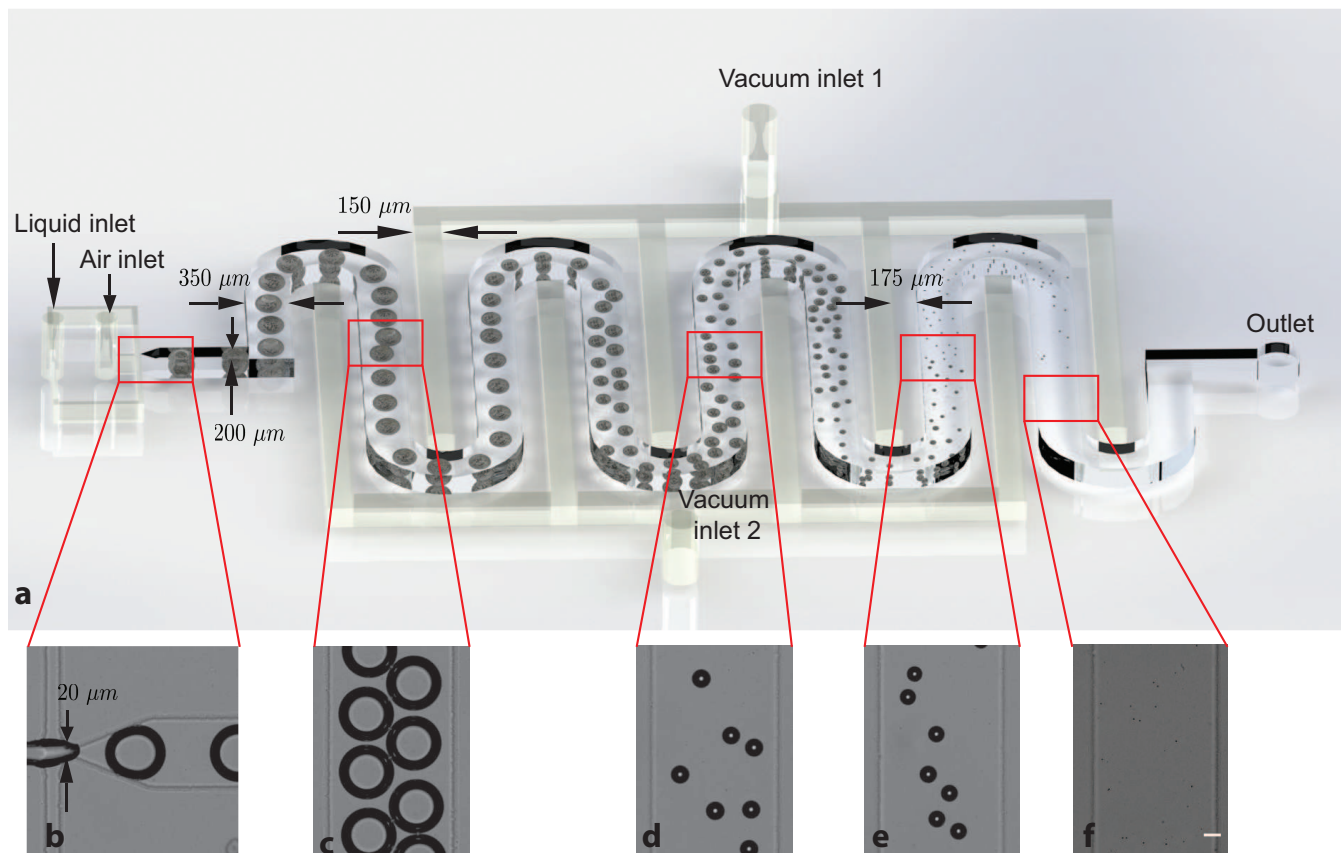


Fig. 1 Our microfluidic device for microbubble generation and shrinking. (a) The three dimensional (3D) schematic diagram shows that bubbles are (b) generated at the orifice and (c-f) shrink as they flow downstream in the serpentine microchannel. Two sets of vacuum channels are embedded adjacent to the serpentine channel. Vacuum inlets 1 and 2 connect the vacuum source to the vacuum microchannels. Representative experimental images (b - f) show the sequential shrinking of the microbubbles in the microchannel. These experimental images are taken from an experiment where the vacuum pressure, $P_v = -50$ kPa. Scale bar represents $50 \mu\text{m}$.

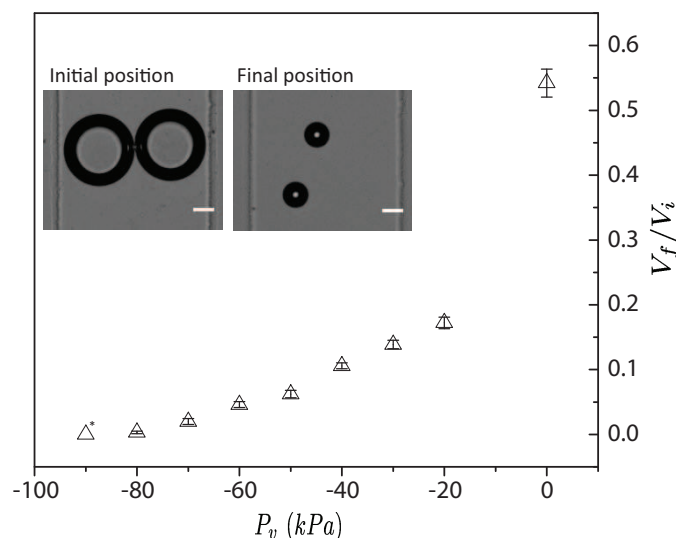


Fig. 2 A plot of the normalized final microbubble volume (V_f/V_i) versus the applied vacuum channel pressure, P_v , in the vacuum microchannels. These experimental results show that, even in the absence of an applied vacuum pressure, the microbubbles shrink to approximately 55 % of their initial volume when flowing through the long serpentine channel. When a vacuum pressure is applied to the vacuum microchannels, we observe that the microbubbles in the serpentine microchannel shrink more dramatically, and their shrinkage increases monotonically with increasing magnitude of the applied vacuum pressure. Here, error bars represent one standard deviation of 10 samples. The insets show representative experimental images of microbubbles at the initial and final positions in the serpentine microchannel, corresponding to microbubble volumes V_i and V_f , respectively. The datum indicated by *** corresponds to the final microbubble volume V_f/V_i from the experiment where the vacuum pressure is $P_v = -90$ kPa. Here, the microbubbles are not visible under the microscope, so we define their volume $V_f/V_i = 0$. The inset images are from an experiment where the vacuum pressure $P_v = -50$ kPa. Scale bars represent 50 μm .

Information.[†]

Fig. 1b shows the orifice where the bubbles are initially generated in the microchannel. The size of these bubbles are known to depend on the size of the orifice, inlet air pressure, liquid-air surface tension, and the continuous liquid flowrate.²² In our experiments, the orifice size, inlet air pressure, liquid-air surface tension, and continuous liquid flow rate are all held constant as described above. Therefore, the initial microbubble volume, $V_i = 1.5$ nL, which we measure immediately downstream of the orifice, is approximately the same in all of our experiments.

Fig. 2 shows a plot of the normalized final microbubble volume, V_f/V_i , versus the applied vacuum pressure, P_v , in the vacuum microchannels. Here, the final microbubble volume, V_f , measured at a fixed location near the outlet for all experiments in the serpentine microchannel, is normalized by the initial volume, V_i , which is measured immediately downstream of the bubble-generating orifice. The inset of Fig. 2 shows two representative images of the microbubbles at the initial and final measurement locations, corresponding to initial and final volumes V_i and V_f , respectively.

We observe that when the applied vacuum pressure, $P_v = 0$, the final microbubble volume V_f is approximately 55 % of the initial

microbubble volume, V_i . We hypothesize that this microbubble shrinking effect, in the absence of an applied vacuum pressure, is due to the high pressure of the gas and liquid in the microchannel, which is a result of the pressure-driven nature of the flows. The pressure in the microchannel is higher than atmospheric pressure, so according to Henry's law, the molecular components of air in the microbubbles will become more soluble in the continuous liquid. This observation of shrinking microbubbles is consistent with the observation of Cubaud et al. who find that carbon dioxide microbubble diameters decrease by as much as 55 % in a 10 cm long serpentine microchannel.³³ Convective liquid-gas mass transfer due to the moving microbubbles may also contribute to microbubbles shrinking along the serpentine microchannel.³⁴ We note, however, that these earlier demonstrations of passive dissolution of gas into the continuous liquid phase is a slow process, so relying on this passive mechanism alone is not sufficient to rapidly generate $O(1)$ μm diameter microbubbles.³⁵

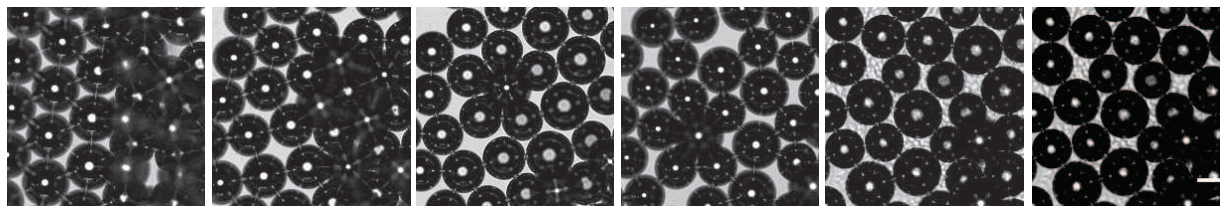
The results in Fig. 2 also show that there is a monotonic decrease in final microbubble volumes, V_f/V_i , with increasing magnitude of the applied vacuum pressure, P_v . This evidence suggests that the applied vacuum pressure P_v , which is easily tunable, is a good control parameter for the resulting microbubble size. Importantly, we are able to shrink the microbubbles to diameters ($D_f = 1-7$ μm) that are desirable to biomedical ultrasound and therapeutics applications.

In our approach, we create a negative pressure (i.e. vacuum) environment in the interdigitated vacuum microchannels that are adjacent to the main serpentine microchannel. Since we do not degas the continuous liquid phase before starting an experiment, the liquid is initially saturated with dissolved components of air at atmospheric pressure. However, PDMS is permeable to various components of air, namely gaseous oxygen, nitrogen, and carbon dioxide.³⁶ Therefore, we hypothesize that, in the microfluidic device, the negative pressure in the vacuum microchannels cause gaseous components of air that are originally dissolved in the liquid continuous phase in the main serpentine channel, to permeate through the PDMS wall,^{36,37} and exit via the vacuum microchannels. Simultaneously, the air inside the microbubbles dissolve into the liquid continuous phase as the bubble-liquid system attempts to continuously attain thermodynamic equilibrium—leading the microbubbles to shrink.

The resulting microbubbles after shrinkage are stable. The shrinking process removes molecules of air from the microbubbles, instead of, for example, compressing the microbubbles in a high pressure environment. Therefore, the microbubbles remain in a thermodynamic equilibrium state in the continuous liquid phase even after returning to an atmospheric pressure environment.

Figs. 3a and 3b show representative experimental images of the microbubbles collected at the outlet of the microfluidic device observed using 10x and 63x microscope objectives, respectively, at different points in time. In Fig. 3a, the microbubbles are from the control experiment where the vacuum pressure, $P_v = 0$ kPa. Fig. 3b shows microbubbles from an experiment where the vacuum pressure is set to $P_v = -70$ kPa. We define the initial time $t=0$ min as the moment when the sample is first collected from the out-

a Control



b $P_v = -70$ kPa

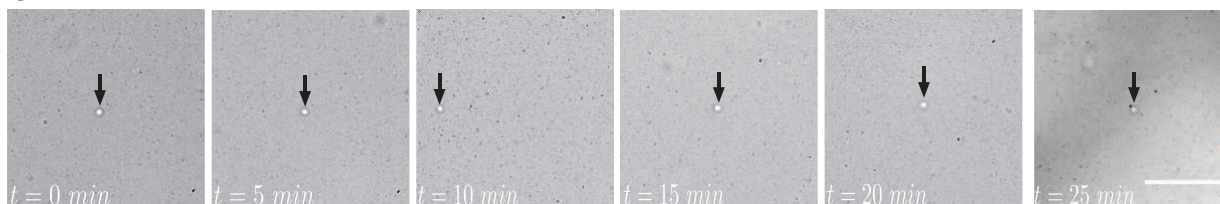


Fig. 3 Representative sequential images of microbubbles collected at the outlet of the microfluidic device. (a) Microbubbles in the control experiment where the applied vacuum pressure, $P_v = 0$ kPa, observed via a 10x objective. (b) Microbubbles generated by a vacuum pressure, $P_v = -70$ kPa, observed with a 63x objective. Here, arrows indicate the position of representative microbubbles in the sample. The microbubble shown in each frame may not be the same due to difficulties tracking the moving bubbles, but all microbubbles had diameter, $D_f = 1 - 7 \mu\text{m}$. Image frames are at 5 minute intervals for both (a) and (b). Scale bars represent $50 \mu\text{m}$.

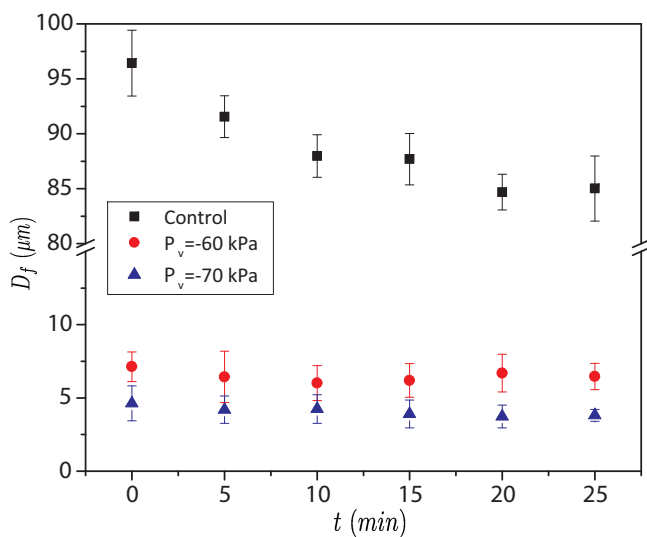


Fig. 4 A plot of the diameter D_f of the collected microbubbles versus time t . The data shown are from three representative experiments using vacuum pressures of $P_v = 0, -60,$ and -70 kPa. Error bars represent one standard deviation for 10 samples.

let. Subsequent sequential images are taken at intervals of 5 min apart. For this particular experiment, the vacuum pressure of $P_v = -70$ kPa results in microbubbles with diameters, D_f , in the range of $1-7 \mu\text{m}$. Both sets of images in Fig. 3 show that the collected microbubbles approximately maintain their size-stability even after 25 min.

Fig. 4 is a plot of the diameter, D_f , of collected microbubbles, versus time t . Here, we report data from three experiments where the applied vacuum pressure $P_v = 0, -60,$ and -70 kPa. The plot shows that, for the control experiment, where $P_v = 0$ kPa, the diameter D_f of the microbubbles decreases by approximately 10

% over a period of 25 minutes. Microbubble diameters D_f remain very stable for the experiments where the applied vacuum pressures $P_v = -60$ and -70 kPa. Critically, this result is evidence that our microfluidic approach for vacuum-shrinking microbubbles is capable of making stable microbubbles that are in relevant length-scale of $1 - 7 \mu\text{m}$ diameter.^{5,17}

For the first time, we demonstrate a microfluidic technique to reduce the size of microbubbles by applying vacuum pressure in interdigitated microchannels that are adjacent to the microchannels containing the flow of a bubble suspension. By tuning a single parameter, the applied vacuum pressure, our approach shrinks microbubbles to the $1 - 7 \mu\text{m}$ diameter relevant length-scale that is desirable in biomedical ultrasound and therapeutics applications. Using this method, we show that microbubbles which are originally more than $100 \mu\text{m}$ in diameter can be reduced to a few micrometers in diameter by controlling the applied vacuum pressure. We also show that the resulting microbubbles remain stable in atmospheric condition for at least 25 minutes.

SSH Tsai, R Karshafian, and MC Kolios acknowledge funding support from the Natural Sciences and Engineering Research Council (NSERC) Discovery grants program. SSH Tsai is also grateful for support from an NSERC Engage grant (grant no. EGP 491921-15) held in collaboration with the industrial partner, MD Precision Inc.

References

- 1 M. J. K. Blomley, J. C. Cooke, E. C. Unger, M. J. Monaghan and D. O. Cosgrove, *British Medical Journal*, 2001, **322**, 1222–1225.
- 2 M. Postema and G. Schmitz, *Ultrasonics Sonochemistry*, 2007, **14**, 438–444.
- 3 S. Qin, C. Caskey and K. Ferrara, *Physics in medicine and biology*, 2009, **54**, 1–42.
- 4 P. a. Dayton, K. E. Morgan, a. L. Klibanov, G. H. Brandenburger and K. W. Ferrara, *IEEE Transactions on Ultrasonics, Ferroelectrics, and Frequency Control*, 1999, **46**, 220–232.
- 5 J. Ma, C. Xu, F. Gao, M. Chen, F. Li and L. Du, *Molecular Medicine Reports*, 2015, **12**, 4022–4028.

- 6 J. E. Streeter, R. Gessner, I. Miles and P. A. Dayton, *Molecular Imaging*, 2010, **9**, 87–95.
- 7 S. Sirsi and M. Borden, *Bubble Science, Engineering and Technology*, 2010, **1**, 3–17.
- 8 R. V. Shohet, S. Chen, Y. T. Zhou, Z. Wang, R. S. Meidell, R. H. Unger and P. a. Grayburn, *Circulation*, 2000, **101**, 2554–2556.
- 9 E. C. Unger, T. O. Matsunaga, T. McCreery, P. Schumann, R. Sweitzer and R. Quigley, *European Journal of Radiology*, 2002, **42**, 160–168.
- 10 E. Stride and M. Edirisinghe, *Medical and Biological Engineering and Computing*, 2009, **47**, 809–811.
- 11 R. Karshafian, S. Samac, P. D. Bevan and P. N. Burns, *Ultrasonics*, 2010, **50**, 691–697.
- 12 P. Marmottant and S. Hilgenfeldt, *Nature*, 2003, **423**, 153–156.
- 13 F. Fekri, R. C. Delos Santos, R. Karshafian and C. N. Antonescu, *PLoS ONE*, 2016, **11**, 1–22.
- 14 N. Rapoport, Z. Gao and A. Kennedy, *Journal of the National Cancer Institute*, 2007, **99**, 1095–1106.
- 15 Z. Gao, A. M. Kennedy, D. A. Christensen and N. Y. Rapoport, *Ultrasonics*, 2008, **48**, 260–270.
- 16 J. R. Lindner, *Nature Reviews Drug Discovery*, 2004, **3**, 527–533.
- 17 H. Lin, J. Chen and C. Chen, *Medical and Biological Engineering and Computing*, 2016, **54**, 1–14.
- 18 E. Stride and M. Edirisinghe, *Soft Matter*, 2008, **4**, 2350–2359.
- 19 K. Bjerknes, K. Dyrstad, G. Smistad and I. Agerkvist, *Drug Development and Industrial Pharmacy*, 2000, **26**, 847–56.
- 20 M. Kukizaki and M. Goto, *Colloids and Surfaces A: Physicochemical and Engineering Aspects*, 2007, **296**, 174–181.
- 21 U. Farook, H. B. Zhang, M. J. Edirisinghe, E. Stride and N. Saffari, *Medical Engineering and Physics*, 2007, **29**, 749–754.
- 22 K. Hettiarachchi, E. Talu, M. L. Longo, P. a. Dayton and A. P. Lee, *Lab on a chip*, 2007, **7**, 463–468.
- 23 M. Seo, R. Williams and N. Matsuura, *Lab on a chip*, 2015, **15**, 3581–3590.
- 24 A. H. Dhanaliwala, J. L. Chen, S. Wang and J. A. Hossack, *Microfluidics and Nanofluidics*, 2013, **14**, 457–467.
- 25 H. Chen, J. Li, W. Zhou, E. G. Pelan, S. D. Stoyanov, L. N. Arnaudov and H. A. Stone, *Langmuir*, 2014, **30**, 4262–4266.
- 26 S. A. Peyman, J. R. McLaughlan, R. H. Abou-Saleh, G. Marston, B. R. Johnson, S. Freear, P. L. Coletta, A. F. Markham and S. D. Evans, *Lab on a Chip*, 2016, **16**, 679–687.
- 27 C. Lochovsky, S. Yasotharan and A. Günther, *Lab on a Chip*, 2012, **12**, 595.
- 28 <http://www.definityimaging.com/main.html>, Accessed: 2017-03-08.
- 29 E. Y. Arashiro and N. R. Demarquette, *Materials Research*, 1999, **2**, 23–32.
- 30 P. S. Sheeran, Y. Daghighi, K. Yoo, R. Williams, E. Cherin, F. S. Foster and P. N. Burns, *Ultrasound in Medicine and Biology*, 2016, **42**, 795–807.
- 31 Y. Xia and G. M. Whitesides, *Annual Review of Materials Science*, 1998, **28**, 153–184.
- 32 B.-U. Moon, D. K. Hwang and S. S. H. Tsai, *Lab on a Chip*, 2016, **8**, 198–220.
- 33 T. Cubaud, M. Sauzade and R. Sun, *Biomechanics*, 2012, **6**, 1–9.
- 34 S. Shim, J. Wan, S. Hilgenfeldt, P. D. Panchal and H. A. Stone, *Lab on a Chip*, 2014, **14**, 2428–36.
- 35 D. J. Cox and J. L. Thomas, *Ultrasound in Medicine and Biology*, 2013, **39**, 466–474.
- 36 T. C. Merkel, V. I. Bondar, K. Nagai, B. D. Freeman and I. Pinnau, *Journal of Polymer Science Part B: Polymer Physics*, 2000, **38**, 415–434.
- 37 L. Xu, H. Lee, D. Jetta and K. W. Oh, *Lab on a Chip*, 2015, **15**, 3962–3979.